JGR Oceans

RESEARCH ARTICLE
10.1029/2022JC018669

Estuarine Salinity Response to Freshwater Pulses

Bouke Biemond[1], Huib E. de Swart[1], Henk A. Dijkstra[1], and Manuel Díez-Minguito[2]

[1]Department of Physics, Institute for Marine and Atmospheric research Utrecht, Utrecht University, Utrecht, The Netherlands, [2]Environmental Fluid Dynamics Group, Andalusian Institute for Earth System Research, University of Granada, Granada, Spain

Key Points:

- Modeling of salt dynamics during strong freshwater pulses requires a detailed description of the vertical structure of salinity
- Dependence of salt intrusion length is quantified from the pulse duration and ratio of river discharge before and during a pulse
- The recovery time after a freshwater pulse does not depend on the change in salt intrusion length induced by the pulse

Supporting Information:

Supporting Information may be found in the online version of this article.

Correspondence to:

B. Biemond,
w.t.biemond@uu.nl

Citation:

Biemond, B., de Swart, H. E., Dijkstra, H. A., & Díez-Minguito, M. (2022). Estuarine salinity response to freshwater pulses. *Journal of Geophysical Research: Oceans*, *127*, e2022JC018669. https://doi.org/10.1029/2022JC018669

Received 24 MAR 2022
Accepted 31 OCT 2022

Abstract

Freshwater pulses (during which river discharge is much higher than average) occur in many estuaries and strongly impact estuarine functioning. To gain insight into the estuarine salinity response to freshwater pulses, an idealized model is presented. With respect to earlier models on the spatiotemporal behavior of salinity in estuaries, it includes additional processes that provide a more detailed vertical structure of salinity. Simulation of an observed salinity response to a freshwater pulse in the Guadalquivir Estuary (Spain) shows that this is important to adequately simulate the salinity structure. The model is used to determine the dependency of the estuarine salinity response to freshwater pulses for different background discharge, tides, and different intensities and durations of the pulses. Results indicate that the change in salt intrusion length due to a freshwater pulse is proportional to the ratio between peak and background river discharge and depends linearly on the duration of the pulse if there is no equilibration during the pulse. The adjustment time, which is the time it takes for the estuary to reach equilibrium after an increase in river discharge, scales with the ratio of the change in salt intrusion length and the peak river discharge. The recovery time, that is, the time it takes for the estuary to reach equilibrium after a decrease in river discharge, does not depend on the amount of decrease in salt intrusion length caused by the pulse. The strength of the tides is of minor importance to the salt dynamics during and after the pulse.

Plain Language Summary

The salinity distribution in an estuary, the transition area between river and sea, strongly depends on the river discharge. During periods of low river discharge, salt will move upstream, but when river discharge becomes high, salt is pushed downstream. This study focuses on the effect of freshwater pulses (short periods with sudden high river discharge) on estuarine salt intrusion. When applying an existing model to observed freshwater pulses in the Guadalquivir Estuary (Spain), it turned out that this model was not able to simulate the effect of strong pulses. A new model has been developed that performs well when being applied to the same situations. With this new model, it is shown that the intensity and duration of the pulse control the decrease in salt intrusion. The strength of the tides is found to be of minor importance. The time it takes before the salt intrusion has recovered to its initial location is determined by the river discharge after the pulse and does not depend on how much the salt intrusion moved downstream.

1. Introduction

Freshwater pulses, here defined as events during which the freshwater discharge by rivers exceeds 3 times its long-yearly average value and which last no longer than 1 month, are common features in many estuaries around the world. They are mostly the result of strong precipitation in the upstream river catchment area (Du & Park, 2019; Du et al., 2019; Gong et al., 2007; Guerra-Chanis et al., 2021; Liu et al., 2008; Tee & Lim, 1987; Valle-Levinson et al., 2002), opening of a freshwater reservoir (Ingram et al., 1986; Lepage & Ingram, 1988), or a combination of those two (Díez-Minguito et al., 2013). The increased freshwater discharge causes a strong downstream transport of salt, which has a large impact on the ecology in the estuary and on the agriculture of the lands around the estuary (McFarland et al., 2022; Paerl et al., 2006). All the above-cited studies indicate that the adjustment time, here defined as the time during which the salinity in an estuary adjusts to high river discharge, is in the order of 1–2 days. Observational studies report that freshwater pulses can cause the salt intrusion length, which is defined as the distance of the 2 psu isohaline to the estuary mouth (Monismith et al., 2002), to shift by tens of kilometers (Díez-Minguito et al., 2013). An estuary can even become entirely fresh (Du & Park, 2019). After such pulses, the estuary returns to its non-disturbed state. Values of the recovery time, defined as the time it takes for the salt intrusion length to reach its background value again, widely vary, but typically they are considerably larger than values of the preceding adjustment times. For example, Valle-Levinson et al. (2002) found

10 days for the Chesapeake Bay (USA), while Gong et al. (2007) reported 4 months for York River estuary, which is located in the same area.

The overall aim of this study is to gain a more detailed understanding of how an estuary will respond to freshwater pulses with different intensity and duration. For such purposes, it is helpful to employ idealized models, which only represent the most dominant physical processes and assume a simplified geometry. Besides yielding insight into the dynamics, these models are fast, flexible, and are thus suitable for extensive sensitivity analysis. Earlier studies on estuarine physics (Chatwin, 1976; Geyer & MacCready, 2014; Hansen & Rattray, 1965; MacCready, 2004) have demonstrated the added value of idealized models with respect to detailed numerical models.

The current knowledge of estuarine adjustment to changes in river discharge originates from both simplified and more sophisticated numerical models and observations. Kranenburg (1986) demonstrated, by using analytical arguments applied to a one-dimensional model, that the response time scale, that is, the time during which an estuary responds to a decrease or increase in river discharge, is inversely proportional to the river discharge after the change. This finding explains the difference between adjustment time and recovery time. Hetland and Geyer (2004) used a three-dimensional primitive equation model with idealized geometry and simple turbulence formulations to study response time scales. They found a clear difference between adjustment and recovery time, which is in line with the finding of Kranenburg (1986). They argued that during net upstream transport of salt, the motion of the salt intrusion adds constructively to the (subtidal) bottom layer flow. This means that velocities in the bottom layer are stronger than during net downstream transport, so import of salt will experience stronger resistance from the bottom drag and will thus be slower than net export of salt. Chen (2015) extended the analysis of Kranenburg (1986) by allowing the density-driven flow in his model to be time-dependent. He argued that the difference between adjustment and recovery time is the result of the nonlinear response of salt intrusion length to changes in river discharge. Monismith (2017) employed a modified version of the model of Chen (2015) to study the unsteadiness of the salt intrusion length under different time-dependent forcings. His model showed good skill in hindcasting salt-intrusion lengths in the northern part of San Francisco Bay.

These studies yielded important insights into the time scales associated with the response of salt intrusion to changes in river discharge. Important to mention here is that the idealized models for estuarine adjustment assume that creation of salinity stratification by vertically sheared velocity is balanced by destruction of stratification by vertical mixing. This assumption is based on Pritchard (1954), who analyzed observations in the James River estuary under relatively low river discharge. Hereafter, we will refer to this balance of processes determining the stratification as the Pritchard balance. Studies by MacCready (2007) and Ralston et al. (2008) demonstrated that this assumption works quite well in cases that they consider, but these cases do not include strong freshwater pulses. Dijkstra and Schuttelaars (2021) showed that in steady state the Pritchard balance does not hold in the high-discharge regime. It may be expected that this is also true for time-dependent cases. Knowledge gaps also exist with regard to the sensitivity of the response of the estuary to freshwater pulses for different environmental settings, for example, different strengths of tides.

The specific aims of this study are twofold. The first is to show the limitations of the Pritchard balance when investigating strong freshwater pulses. The second is to investigate the sensitivity of the estuarine salinity response to a freshwater pulse to different parameters. We quantify the estuarine salinity response by calculating adjustment time scales, recovery time scales, and changes in salt intrusion lengths. There are three research questions associated with this second aim: (1) what is the effect of the background conditions of the estuary, that is, the background river discharge and the strength of the tides, on the salinity response? (2) What is the effect of the strength of the peak river discharge on the salinity response? (3) What is the effect of the duration of the pulse on the salinity response?

The remaining of this paper is organized as follows: In Section 2.1, deficiencies, including negative salinity values, are identified when the model of MacCready (2007) (MC07 hereafter), which uses the Pritchard balance, is forced with observed river discharge during a strong freshwater pulse in the Guadalquivir Estuary (Spain). A new model, which builds on MC07 but does not rely on the Pritchard balance, is presented in Section 2.2. This model does not have the deficiencies of MC07 when used to simulate freshwater pulses in the Guadalquivir Estuary (Section 2.3). Afterward, a sensitivity analysis is done in a more idealized model setup. The experimental setup is given in Section 2.4, followed by the results and discussion (Section 3) and the conclusions (Section 4).

2. Material and Methods

2.1. Limitations of the Pritchard Balance

In order to show the limitations of available idealized models for estuarine adjustment, the MC07 model is used to simulate the estuarine response to an observed strong freshwater pulse. This model simulates time-dependent, tidally averaged, width-averaged estuarine flow and salinity, building on Hansen and Rattray (1965). The vertical momentum balance is hydrostatic, while in the horizontal a balance is assumed between the pressure gradient force and internal friction. Furthermore, the Pritchard balance is used to describe the vertical structure of salinity. The MC07 model is here applied to the freshwater pulse in February 2009 in the Guadalquivir Estuary (Díez-Minguito et al., 2013; Losada et al., 2017; Wang et al., 2014). This pulse has a maximum discharge (main river + tributaries) of 889 $m^3\ s^{-1}$, while the river discharge in the month before the pulse has an average value of about 32.3 $m^3\ s^{-1}$. The model settings are as follows: the estuary is 110 km long and its width increases exponentially from 150 m at the upstream limit to 650 m at the mouth. The thalweg has an average depth of 7.1 m (Díez-Minguito et al., 2013), so this is used as the depth of the estuary. The vertical eddy-viscosity coefficient, vertical eddy-diffusion coefficient, and horizontal eddy-diffusion coefficient are chosen as in Ralston et al. (2008) and Guha and Lawrence (2013). This means that they depend on the strength of the tidal current and a turbulent length scale, which is the estuary depth for the vertical coefficients and the estuary width for the horizontal coefficient. The model is forced with the observed river discharge from the Alcala del Rio dam and from the four main tributaries after this dam: Aznalcázar, El Gergal, Guadaíra, and the Torre del Águila (Agencia de Medio Ambiente y Agua de Andalucía, see chguadalquivir.es/saih/Inicio.aspx). The representative tidal current amplitude is based on measurements (Navarro et al., 2011) and set to be 1.15 m s^{-1} and the ocean salinity is 35 psu. The horizontal grid size is 250 m and a time step of 15 s is used to ensure numerical stability.

Results from this simulation are displayed in Figures 1a and 1b. Before the pulse, the salinity field is only slightly disturbed by the variations in river discharge. During the freshwater pulse, surface salinity values drop and within a few days after the start of the pulse they reach values of −4.7 psu close to the mouth. The minimum value for surface salinity is thus below zero. Note that at the same time, bottom salinity values at the estuary mouth are prescribed to be 35 psu, which means that the estuary is strongly stratified during the pulse in this simulation. After the pulse, negative salinity values disappear. Salt intrusion recovers in about 3 weeks to values comparable to the ones before the pulse. The negative values of surface salinity during the pulse are unphysical and motivated the development of a new model that is presented in the next section.

2.2. Model Formulation

2.2.1. Domain

The study area consists of two parts: an estuary and the adjacent sea. We use x as the along-channel coordinate, where $x = -L_e$ is the upstream limit, $x = 0$ is the estuary mouth, and $x = L_s$ is the boundary of the adjacent sea. The width of the estuary is

$$b(x) = b_0 \exp\left(\frac{x + L_e}{L_b}\right), \tag{1}$$

where b_0 is the width at the upstream limit and L_b is the e-folding length scale which controls the width convergence. The estuary and the open sea have different values of L_b; the depth H is constant throughout the domain.

2.2.2. Hydrodynamic Module

The hydrodynamic equations are identical to those in MC07. The equations are averaged over the cross-channel y-coordinate and over the tides. Wind is ignored and the Boussinesq approximation is used, with an equation of state that expresses a linear relation between variations in salinity and variations in density. The only difference with respect to MC07 concerns the boundary condition at the bottom $z = -H$, which is taken to be a partial slip condition (instead of no-slip), as in Dijkstra and Schuttelaars (2021), and reads

$$A_v \frac{\partial u}{\partial z} = S_f u \quad \text{at} \quad z = -H. \tag{2}$$

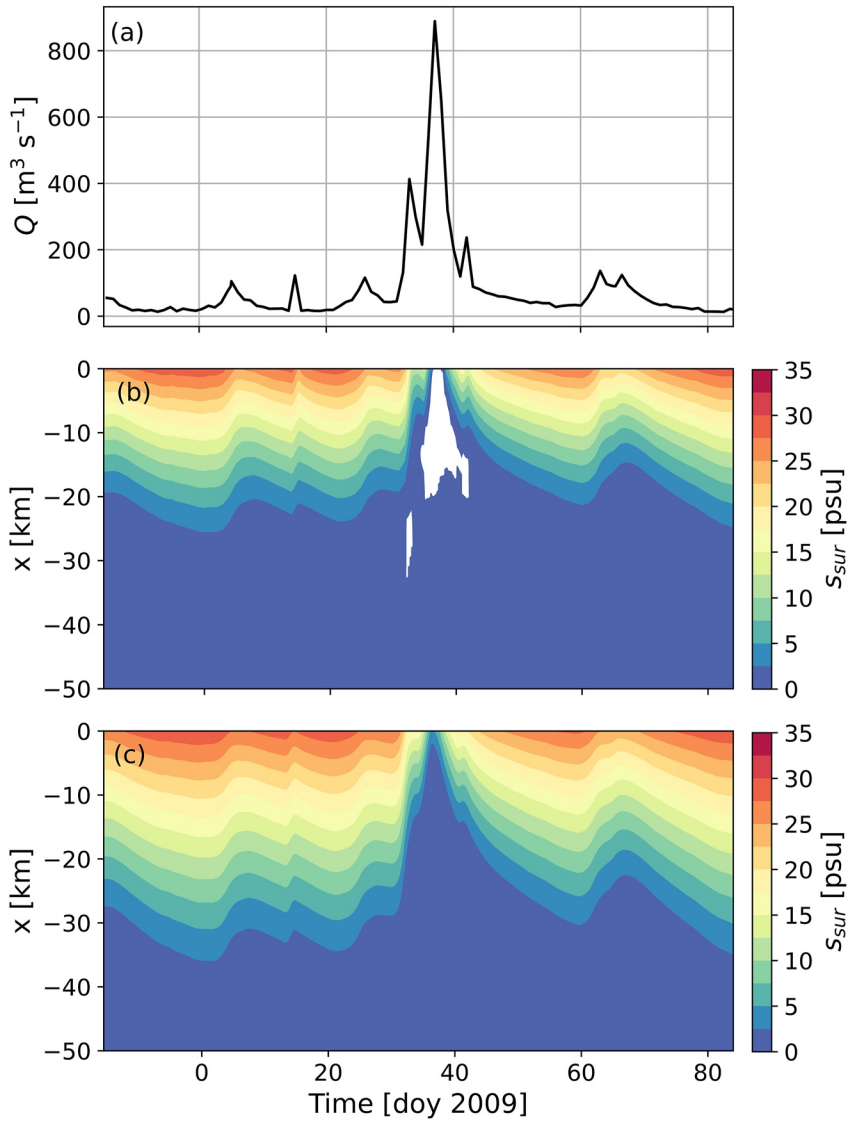

Figure 1. Application of two different models for the case of an observed freshwater pulse in the Guadalquivir Estuary in February 2009. (a) Time series of observed river discharge. (b) Simulated surface salinity s_{sur} with the MacCready (2007) model, which uses the Pritchard balance, versus time and along-channel coordinate x, where $x = 0$ is the estuary mouth. The white area indicates where s_{sur} is negative. (c) As (b), except for the simulation with the model presented in Section 2.2.

Here, $S_f = \frac{2A_v}{H}$ is the friction coefficient, A_v is the vertical eddy-viscosity coefficient (assumed constant, see later), u is the along-channel velocity, and z is the vertical coordinate. At the upstream limit, a river discharge Q is imposed:

$$b_0 \int_{-H}^{0} u \; dz = Q \quad \text{at} \quad x = -L_e. \tag{3}$$

The along-channel velocity u and salinity s are split in their respective depth-averaged parts (denoted by a bar) and depth-dependent parts (denoted by primes):

$$u = \bar{u} + u', \quad s = \bar{s} + s'. \tag{4}$$

The solutions of the equations for along-channel velocity read

$$\bar{u} = \frac{Q}{bH}, \quad u' = \bar{u}\left(\frac{1}{5} - \frac{3}{5}\frac{z^2}{H^2}\right) + \alpha\frac{\partial \bar{s}}{\partial x}\left(\frac{8}{5} - \frac{54}{5}\frac{z^2}{H^2} - 8\frac{z^3}{H^3}\right), \tag{5}$$

where $\alpha = \frac{g\beta H^3}{48A_v}$. Here, $g = 9.81$ m s^{-2} is gravitational acceleration and β the isohaline contraction coefficient of water (=7.6×10^{-4} psu^{-1}). The vertical eddy-viscosity coefficient is parametrized as $A_v = c_v U_T H$, where U_T is the amplitude of the tidal current and $c_v = 7.28 \times 10^{-5}$ is an empirical constant (Ralston et al., 2008). This formulation is based on the assumption that the relevant velocity scale for turbulent mixing in an estuary is the amplitude of the tidal current and the limiting vertical length scale of the turbulent eddies is the depth of the estuary. The physical interpretation of Equation 5 is that the depth-averaged current is solely due to the river discharge and that the vertical velocity shear is caused by the river current and the density-driven flow. Hereafter, we will refer to u' as the exchange flow (Geyer & MacCready, 2014). The vertical velocity w follows from continuity,

$$\frac{\partial}{\partial x}(bu) + \frac{\partial}{\partial z}(bw) = 0, \tag{6}$$

which results in

$$w = \alpha H \left(\frac{\partial^2 \bar{s}}{\partial x^2} + L_b^{-1}\frac{\partial \bar{s}}{\partial x}\right)\left(2\frac{z^4}{H^4} + \frac{18}{5}\frac{z^3}{H^3} - \frac{8}{5}\frac{z}{H}\right). \tag{7}$$

2.2.3. Salt Module

The salt conservation equation is

$$\frac{\partial s}{\partial t} + \frac{1}{b}\frac{\partial}{\partial x}(bus) + \frac{\partial}{\partial z}(ws) = \frac{1}{b}\frac{\partial}{\partial x}\left(bK_h\frac{\partial s}{\partial x}\right) + \frac{\partial}{\partial z}\left(K_v\frac{\partial s}{\partial z}\right), \tag{8}$$

where t is time. The horizontal eddy-diffusion coefficient is parametrized as $K_h = c_h U_T b$, where $c_h = 0.035$ is an empirically determined constant (Banas et al., 2004). A closure relation for the vertical eddy-diffusion coefficient K_v is $K_v = \frac{A_v}{Sc}$, with $Sc = 2.2$ the Schmidt number (Ralston et al., 2008). At the upstream limit ($x = -L_e$), a river salinity s_{ri} imposed. The simulated domain stretches well beyond the limit of salt intrusion, to avoid that this condition affects the salinity dynamics in the estuary. In the part that represents the adjacent sea, width increases strongly with distance to the mouth, so that the river flow will become very weak at the sea boundary $x = L_s$. This allows us to assume that at this downstream boundary of the domain (located seaward of the estuary mouth at $x = 0$), salinity will be well mixed over the vertical and we can set salinity to be equal to the ocean salinity s_{oc} over the entire depth. Hence,

$$s|_{x=-L_e} = s_{ri} \quad , \quad s|_{x=L_s} = s_{oc}. \tag{9}$$

At the bottom and the free surface the vertical salt flux vanishes:

$$K_v\frac{\partial s}{\partial z} = 0 \quad \text{at} \quad z = -H \ \text{ and } \ z = 0. \tag{10}$$

At the transition between the parts at $x = 0$, both s and the salt transport $b\left(us - K_h\frac{\partial s}{\partial x}\right)$ have to be continuous. Since u and b are continuous, this last condition implies that $\frac{\partial s}{\partial x}$ has to be continuous as well. This can be written as

$$\lim_{x\uparrow 0} s = \lim_{x\downarrow 0} s, \quad \lim_{x\uparrow 0}\frac{\partial s}{\partial x} = \lim_{x\downarrow 0}\frac{\partial s}{\partial x}. \tag{11}$$

2.2.4. Solution Method

To solve for salinity, Equation 4 is inserted into Equation 8 and this equation is averaged over the depth, resulting in the depth-averaged salt balance:

$$\underbrace{\frac{\partial \bar{s}}{\partial t}}_{T_1} + \underbrace{\frac{1}{b}\frac{\partial}{\partial x}(b\bar{u}\bar{s})}_{T_2} + \underbrace{\frac{1}{b}\frac{\partial}{\partial x}\left(b\overline{u's'}\right)}_{T_3} - \underbrace{\frac{1}{b}\frac{\partial}{\partial x}\left(bK_h\frac{\partial \bar{s}}{\partial x}\right)}_{T_4} = 0. \tag{12}$$

Here T_1 is the tendency term. Terms T_2–T_4 contain along-channel variations of three width-integrated and depth-mean salt fluxes: that due to river flow (T_2), due to exchange flow (T_3, which can be split into a contribution

by the density-driven current and a contribution induced by the river current), and a diffusive flux (T_4). The equation for the evolution of s' is found by subtracting Equation 12 from Equation 8, yielding

$$\underbrace{\frac{\partial s'}{\partial t}}_{T_5} + \underbrace{\bar{u}\frac{\partial s'}{\partial x}}_{T_6} + \underbrace{u'\frac{\partial s'}{\partial x}}_{T_7} + \underbrace{u'\frac{\partial \bar{s}}{\partial x}}_{T_8} - \underbrace{\frac{1}{b}\frac{\partial}{\partial x}\left(b\overline{u's'}\right)}_{T_9} + \underbrace{w\frac{\partial s'}{\partial z}}_{T_{10}} - \underbrace{\frac{\partial}{\partial z}\left(K_v\frac{\partial s'}{\partial z}\right)}_{T_{11}} - \underbrace{\frac{1}{b}\frac{\partial}{\partial x}\left(bK_h\frac{\partial s'}{\partial x}\right)}_{T_{12}} = 0. \quad (13)$$

Term T_5 is the tendency term. Terms T_6 and T_7 represent the horizontal advection of s' and T_8 the creation of stratification by vertical velocity shear. Term T_9 is equal to minus T_3, T_{10} represents vertical advection, T_{11} vertical diffusion, and finally T_{12} represents horizontal diffusion. Note that when the Pritchard balance is applied, only terms T_8 and T_{11} are taken into account in Equation 13.

This set of equations is solved for $\bar{s}$ and s'. To deal with the vertical variations, a Galerkin method (see e.g., Canuto et al., 2012) is used. For this, the depth-dependent salinity is written as a Fourier series:

$$s' = \sum_{n=1}^{N} s_n(x,t)\cos\left(\frac{n\pi}{H}z\right), \quad (14)$$

where N is the number of vertical modes and s_n are the Fourier components, which depend on the horizontal coordinate x and on time t. This expression is substituted into Equation 13, and afterwards this equation is projected onto the Fourier modes. Combined with Equation 12, this yields $N + 1$ equations for $\bar{s}(x, t)$ and the $s_n(x, t)$, $n = 1, 2, \ldots, N$, which are numerically solved by using central differences on a spatially uniform grid in x, while time integration is performed with the Crank–Nicolson method (Crank & Nicolson, 1947). This results in a system of $N + 1$ algebraic equations at every grid point, containing values of $\bar{s}$ and s_n at the previous and current time step. This system of equations is solved with the Newton–Raphson method (see e.g., Galántai, 2000).

2.3. Performance of the Model

The new model is subsequently used to simulate the same freshwater pulse in the Guadalquivir Estuary, as was done with the MC07 model. A comparison with observations will be shown in Section. 3.2, here the focus is on whether the model simulates negative salinity values or not. Model settings are the same as in Section 2.1. Additionally, the number of vertical modes is chosen as $N = 10$ and the sea domain is modeled as a 25-km-long channel with an e-folding length scale of 2.5 km. As the numerical scheme is now implicit, it allows for larger time steps. A standard value of $\Delta t = 12$ hr is chosen, but to guarantee accuracy a smaller Δt is chosen when the salt field changes fast. When the change in salinity is large, the Newton–Raphson algorithm may not converge for too large time steps. When this happens, also a smaller time step is chosen; a minimum time step of 15 min is used.

Results from this simulation are displayed in Figure 1c. Before and after the freshwater pulse, salt intrusion is stronger than in the simulation with the MC07 model (Figure 1b). However, during the pulse, no negative values of salinity are simulated, which indicates that our model has overcome the problematic behavior of the MC07 model when simulating strong freshwater pulses. To check the numerical accuracy of the solutions, additional simulations were done where the time and spatial resolution were taken twice as small and with the number of vertical modes increased to $N = 15$. The maximum difference in salinity between the simulations was smaller than 0.01 psu, assuring that the results are sufficiently accurate.

There are three possible explanations for the difference between the MC07 model and the new model: the different boundary condition for momentum at the bottom, the different boundary condition for salinity at the sea boundary (and the inclusion of the sea domain), or the generalized equation for the evolution of s'. First, to determine whether the boundary condition for momentum is the cause, an additional simulation was done where the no-slip boundary condition from MC07 was used as a boundary condition for momentum. In this simulation, salt intrusion before and after the pulse is smaller than in the simulation with the partial slip boundary condition, but no negative salinity values were simulated. Second, the effect of the boundary condition for salinity at the sea boundary was investigated by calculating the value of salinity at the bottom at the estuary mouth. This has a minimum value of 32.8 psu, which is a relatively small (≈10%) deviation from the prescribed value in the MC07 model. Third, the effect of the additional terms in Equation 13 was studied. Figure 2 displays the terms in this equation during the simulation. It is clear that the largest terms during the entire simulation are T_8 (Figure 2d) and

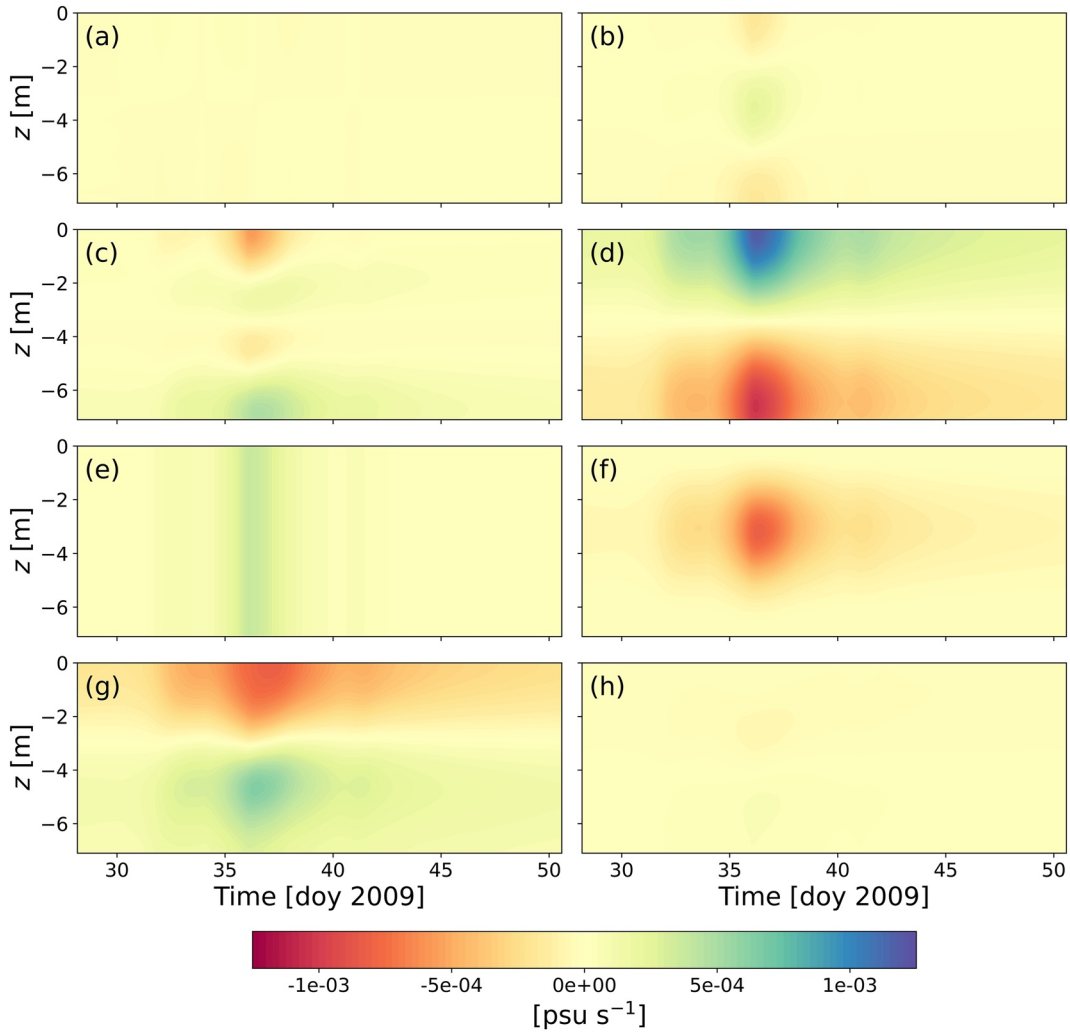

Figure 2. The magnitudes of the different terms in Equation 13 versus time and depth in the first grid cell upstream of $x = 0$ during the simulation of the February 2009 freshwater pulse in the Guadalquivir Estuary with our model. (a) T_5, (b) T_6, (c) T_7, (d) T_8, (e) T_9, (f) T_{10}, (g) T_{11}, and (h) T_{12}.

T_{11} (Figure 2g), which are the only terms taken into account in MC07. However, during the pulse, also other terms become important, in particular T_{10} (Figure 2f), the vertical (upward) advection of salt. This explains why negative salinity can occur in MC07: the amount of destruction of stratification by vertical mixing during freshwater pulses is too small compared to the creation by vertical shear. This leads to an overestimation of stratification in MC07, leading to negative salinity in the surface layer.

2.4. Setup of the Numerical Experiments

Next, the model is used to study the sensitivity of the estuarine salinity response to freshwater pulses. For this, a model domain is chosen that is a straight channel with a width of 1,000 m and a depth of 10 m. The adjacent sea part is 25 km long and it has a convergence length of 2.5 km. This setting is chosen to mimic an "average" coastal plain estuary. Sea salinity is 35 psu and river salinity is 0 psu. The horizontal grid size varies between a minimum of 125 m and maximum of 500 m for different simulations and the number of vertical modes ranges from 5 to 15, depending on the strength of the stratification. The time step has values between 15 min and 24 hr, giving sufficiently accurate solutions. To model a freshwater pulse, an initial state is chosen in which the subtidal estuarine salinity is steady and in equilibrium with the background river discharge Q_{bg}. The pulse starts when the river discharge increases suddenly to its peak value Q_p. The river discharge remains then for a time T_{pulse} at this

peak discharge. After the pulse, the river discharge instantly returns to Q_{bg}. Each simulation is continued until the salt intrusion length has recovered to its initial value. The salt intrusion length X_2 is defined as the distance between the estuary mouth and the most upstream position where the salinity exceeds 2 psu.

To quantify the salinity response to a freshwater pulse, several output quantities are defined: change in salt intrusion length ΔX_2, adjustment time T_{adj}, and recovery time T_{rec}. Change in salt intrusion length ΔX_2 is the difference between the value of the salt intrusion length before the pulse and its minimum value during the pulse. Adjustment time T_{adj} is defined as

$$X_2(t = T_{adj}) = X_2(t = 0) - 0.9\Delta X_2, \tag{15}$$

which is the time it takes for the salinity in the estuary to adjust to the peak river discharge. Recovery time T_{rec} is the time after the pulse when

$$X_2(t = T_{rec}) = X_2(t = 0) - 0.1\Delta X_2, \tag{16}$$

so it is the time when 90% of the recovery of X_2 after the pulse has taken place. These quantities are scaled to make the resulting dependencies more general. As a scale for ΔX_2, the background salt intrusion length $X_2(t = 0)$ is used. We make our adjustment time scale dimensionless with

$$T_{adj,sc} = \frac{0.9bH\Delta X_2}{Q_p}. \tag{17}$$

This formulation is based on the time that a particle would travel over a distance ΔX_2 with the river velocity during the pulse, a quantity that also was considered by Kranenburg (1986). The factor 0.9 accounts for the fact that here T_{adj} is defined when 90% of the change in X_2 has occurred. Finally, T_{rec} is made dimensionless with

$$T_{rec,sc} = \frac{0.9bHX_2(t = 0)}{Q_{bg}}. \tag{18}$$

This is the time scale that results from the assumption that recovery is primarily due to salt transport by the exchange flow. Classical theory (Chatwin, 1976) is applied, that is, $\overline{u's'}$ during the recovery is approximately balanced by salt transport due to river flow. The factor 0.9 is added for the same reason as that in the formulation of $T_{adj,sc}$.

The research questions as formulated in the introduction separated the quantification of the estuarine salinity response to freshwater pulses into three parts: the sensitivity to the background state (research question 1), the sensitivity to the peak river discharge (research question 2), and the sensitivity to the duration of the pulse (research question 3). These different research questions motivate the variation of four dimensional parameters: U_T, Q_{bg}, Q_p, and T_{pulse}. These are converted into four dimensionless parameters, which are Fr_T, $Fr_{R,bg}$, $Fr_{R,p}$, and $\tilde{T}_{pulse}$. Here, $Fr_T = \frac{U_T}{c}$ is the tidal Froude number, with $c = \sqrt{g\beta H s_{oc}}$ an internal velocity scale that equals twice the maximum internal wave speed. Note that Fr_T can also be written as $Ri_L^{-\frac{1}{2}}$, with Ri_L the bulk Richardson number. Furthermore, $Fr_{R,bg} = \frac{Q_{bg}}{bHc}$ is defined as the background freshwater Froude number and $Fr_{R,p} = \frac{Q_p}{bHc}$ the peak freshwater Froude number. Finally, $\tilde{T}_{pulse} = \frac{T_{pulse}}{T_{adj}}$ is the scaled duration of the pulse.

Specifically, for addressing research question 1, a number of simulations is performed where $Fr_{R,p}$ is fixed and Fr_T and $Fr_{R,bg}$ are varied, since these two quantities are shown to determine the equilibrium state of an estuary (Geyer & MacCready, 2014). The duration of the pulse is chosen to exceed the adjustment time, so equilibrium with the peak river discharge is reached during the pulse. This set of simulations will be referred to as experiment set *Background*. For answering research question 2, $Fr_{R,bg}$ and $Fr_{R,p}$ are varied. The tidal Froude number Fr_T is fixed at a value of 0.62 ($U_T = 1$ m s^{-1}). The duration of the pulse T_{pulse} again exceeds the adjustment time. This set of simulations will be referred to as experiment set *Peak*. For addressing research question 3, the duration of the pulse is varied, as well as $Fr_{R,bg}$ and $Fr_{R,p}$. The tidal Froude number Fr_T is again fixed at 0.62. The values of $Fr_{R,bg}$ and $Fr_{R,p}$ are equal to those in set *Peak*. Two series of simulations are done where $\tilde{T}_{pulse} = \frac{1}{2}$ and $\frac{1}{4}$. These simulations will be referred to as experiment set *Short*. Table 1 contains the range of values of the dimensional parameters for all the experiments that were conducted.

Table 1
Amplitude of Tidal Current U_T, Background River Discharge Q_{bg}, Peak River Discharge Q_p, and Duration of the Pulse T_{pulse} for the Different Sets of Experiments

Parameter	*Background*	*Peak*	*Short*
U_T (m s^{-1})	0.75–1.5	1.0	1.0
Q_{bg} (m^3 s^{-1})	16–808	16–1,211	16–1,211
Q_p (m^3 s^{-1})	2,423	323–4,846	323–4,846
T_{pulse}	$>T_{adj}$	$>T_{adj}$	$\frac{1}{4}T_{adj}$, $\frac{1}{2}T_{adj}$

The range of the parameters is based on the following. The amplitude of the tidal current U_T is chosen between 0.75 and 1.5 m s^{-1}, which results in Fr_T ranging from 0.46 to 0.93. Weaker tides are not investigated because the momentum balance relies on the assumption of moderate to strong tidal currents with respect to the river current. Larger tidal currents are not investigated because they are considered to be nonrealistic. The range of values of the freshwater Froude numbers is based on daily discharge values from six estuaries where freshwater pulses are identified. The considered estuaries are the Gironde (France), the Guadiana (Spain/Portugal), the Guadalquivir (Spain), Mitchell River (Australia), San Francisco Bay (USA), and the Tagus (Portugal). Specifics of the river discharge data sets are given in Table 2. Freshwater pulses are identified in the river discharge data sets and displayed in ($Fr_{R,p}$, $Fr_{R,bg}$) parameter space in Figure 3. Based on these observations, a value of $Fr_{R,p} = 0.15$ is chosen as a standard value for the simulations of experiment set *Background*. Since a freshwater pulse is defined here as an event when the river discharge exceeds 3 times its long-yearly average value, an obvious upper bound for $Fr_{R,bg}$ is 0.05 for this set of experiments, one third of the value of $Fr_{R,p}$. The lower bound is $Fr_{R,bg} = 0.001$. For experiment set *Peak*, values of $Fr_{R,bg}$ range from 0.001 to 0.075 and those of $Fr_{R,p}$ range between 0.02 and 0.3. These boundaries are indicated by the black lines in Figure 3. The majority of the observed freshwater pulses fit within these boundaries, but not all of them. Observed pulses for which 3 $Fr_{R,bg} > Fr_{R,p}$ probably started far from a steady state (shortly before the pulse, another pulse occurred) and are thus not considered. The strongest freshwater pulses in the Guadalquivir and Guadiana have $Fr_{R,p} > 0.3$ and are also outside the investigated parameter space. This is done because multiple model assumptions are not valid anymore under such extreme circumstances, in particular the width and depth being constant. Such strong freshwater pulses will increase the water level significantly and flood lands next to the estuary. Moreover, simplifying assumptions regarding the momentum balance, which rely on the estuary being partially to well mixed, do not hold during such extreme events.

3. Results and Discussion

3.1. Sensitivity Analysis

Results of experiment set *Background* are displayed in Figure 4. Panels show the dependence of background salt intrusion length, change in salt intrusion length, adjustment time, and recovery time on the tidal Froude number Fr_T and background freshwater Froude number $Fr_{R,bg}$. Note that intensity and duration of the freshwater pulse are kept fixed (Table 1). Clearly, all dimensional response characteristics (contours in Figure 4) become lower for higher Fr_T and higher $Fr_{R,bg}$. The scaled quantities in Figures 4b–4d show a different behavior: they only weakly depend on Fr_T and for increasing $Fr_{R,bg}$ the relative change in salt intrusion length decreases, while the scaled adjustment and recovery time increase.

Table 2
Specifications of River Discharge Data Sets for Six Estuaries Where Freshwater Pulses Occur

Estuary	Station	Produced by	Period	Width (m)	Depth (m)
Gironde	Lamonzie-Saint-Martin and Tonneins	Banque Hydro	2001–2020	5,000	9
Guadiana	Pulo do Lobo	Portuguese Water Institute	1947–2020	500	6.5
Guadalquivir	Alcalá del Rio dam	Agencia de Medio Ambiente y Agua de Andalucía	1931–2011	500	7.1
San Francisco Bay	Net outflow	California Department of Water Resources	1929–2020	3,000	12
Tagus	Ómnias (Santarém)	Portuguese Water Institute	1972–2002	1,800	5.1
Mitchell River (Queensland)	Koolatah	GRDC data portal	1972–2012	1,000	7

Note. For the Gironde, river discharge from the Garonne and Dordogne are added. For the San Francisco Bay, the data set combines multiple sources. For width and depth, representative values are selected.

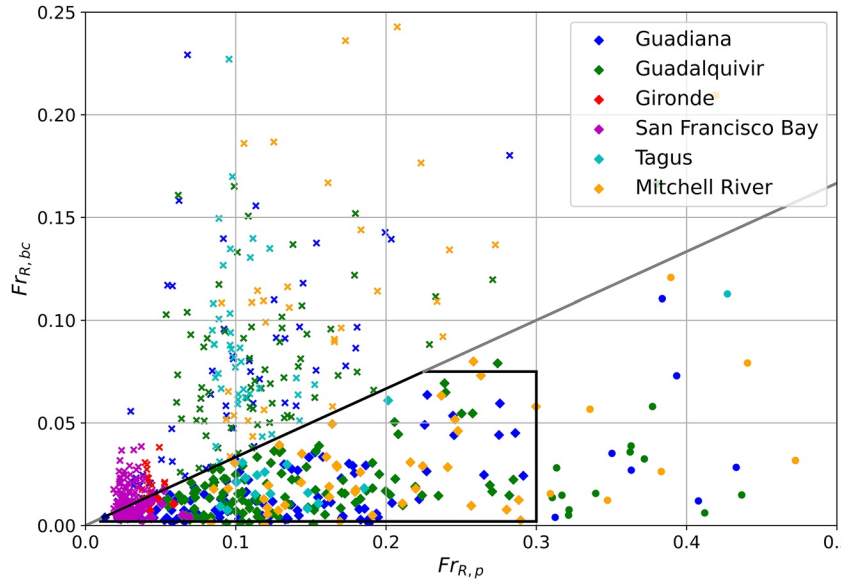

Figure 3. Observed freshwater pulses in the $Fr_{R,p}$, $Fr_{R,bg}$ parameter space. The cross-shaped markers are freshwater pulses where the peak river discharge is less than 3 times the background river discharge, the diamond-shaped markers indicate events where the peak river discharge exceeds this value, and the circular markers indicate freshwater pulses where $Fr_{R,p} > 0.3$. The gray line is where $Fr_{R,p} = 3\ Fr_{R,bg}$. The black box indicates the part of the parameter space that was investigated by experiments *Peak* and *Short*.

Based on classical theory on estuarine salt dynamics (Chatwin, 1976; Geyer & MacCready, 2014; Hansen & Rattray, 1966), one would expect the dependence of background salt intrusion length $X_2(t = 0)$ on Fr_T and $Fr_{R,bg}$ (Figure 4a) to follow the power law relationship:

$$X_2(t = 0) \sim {Fr_{R,bg}}^{-1/3} Fr_T^{-1}. \tag{19}$$

However, for low values of the river flow ($Fr_{R,bg} < 0.005$), horizontal diffusion of salt is important, next to the salt import by exchange flow, and this power law is not valid. Excluding this regime, a least squares fit to the numerical results yields

$$X_2(t = 0) \sim {Fr_{R,bg}}^{-0.39\pm0.0} Fr_T^{-0.98\pm0.01}, \tag{20}$$

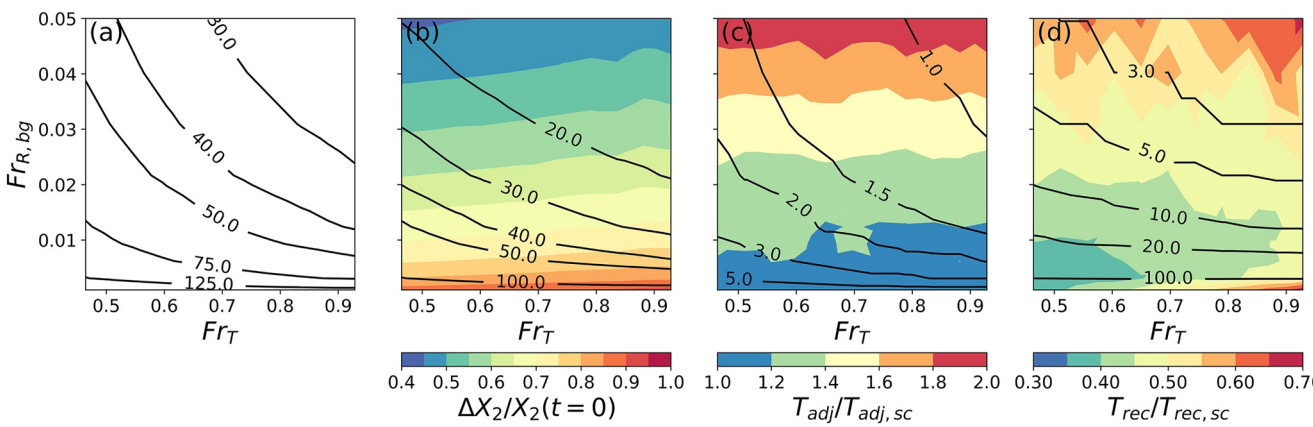

Figure 4. Results of experiment set *Background*. (a) Contour plot of background salt intrusion length $X_2(t = 0)$ (values in km) as a function of tidal Froude number Fr_T and background freshwater Froude number $Fr_{R,bg}$. (b) As panel (a), except for the change in salt intrusion length ΔX_2 (contours, values in km) and the change in the scaled salt intrusion length $\Delta X_2/X_2(t = 0)$ (colors). (c). As panel (b), except for the adjustment time T_{adj} (contours, values in days) and the scaled adjustment time $T_{adj}/T_{adj,sc}$ (colors). (d) As panel (c), except for the recovery time T_{rec} and the scaled recovery time $T_{rec}/T_{rec,sc}$.

with $R^2 = 0.998$, in good agreement with classical theory, which is expected because the model contains the same physics as these models. This theory also explains the patterns found in Figure 4b, as it predicts that

$$\Delta X_2 \sim \left(Fr_{R,p}^{-1/3} - Fr_{R,bg}^{-1/3} \right) Fr_T^{-1}, \tag{21}$$

while a least squares fit to the data yields

$$\Delta X_2 \sim \left(Fr_{R,p}^{-0.28\pm0.00} - Fr_{R,bg}^{-0.31\pm0.01} \right) Fr_T^{-0.89\pm0.01}, \tag{22}$$

with $R^2 = 0.999$. Scatter plots showing the performance of the fits are in Text S1 in Supporting Information S1. Also, it follows that $\Delta X_2/X_2(t = 0)$ is independent of Fr_T.

The patterns shown in Figures 4c and 4d can be understood by identifying and analyzing the processes that act during adjustment and recovery. Figure 4c shows that for $Fr_{R,bg} < 0.015$ the adjustment time $T_{adj} \simeq T_{adj,sc}$. In this "high-pulse regime," where the peak river discharge is relatively large compared to the background river discharge, the dominant process for adjustment is the export of salt by river flow during the pulse. In the "moderate-to-low pulse regime" (the upper part of the panel), T_{adj} is considerably larger than $T_{adj,sc}$. During the adjustment, other salt transport mechanisms are then effective as well, viz. import of salt by both the exchange flow and by horizontal diffusion. As they oppose the salt export by river flow, the adjustment time is larger than that would result from river flow alone. The fact that the value of Fr_T does affect the dimensional adjustment time but not the scaled adjustment time indicates that its effect is mostly through a larger change in salt intrusion length (see Figure 4b), but that the celerity of the adjustment is not sensitive to Fr_T.

A similar reasoning applies to the recovery time: it will be close to the scaled value $T_{rec,sc}$ if the recovery process is controlled by salt transport due to the exchange flow, as described by the classical theory. Figure 4d shows that this only approximately holds in the "weak pulse regime," that is, in the upper part of the diagram. For moderate to stronger pulses, values of the recovery time are approximately half of $T_{rec,sc}$. This deviation from quasi-steady classical theory exists because immediately after the pulse, the landward salt transport due to exchange flow is substantially larger than the seaward transport by river flow. A larger value of Fr_T, that is, stronger tidal mixing, will result in slower recovery, because the magnitude of the exchange flow is inversely proportional to the value of U_T. Yet the recovery time is not very sensitive to the value of U_T because this effect is compensated by the fact that the change in salt intrusion length also decreases approximately linearly for higher U_T.

To look at this in more detail, we present results of the change in salt content of an estuary for different values of the background river discharge and of the tidal current amplitude. The integrated salt balance is obtained by integrating Equation 12 over the volume of the estuary:

$$\underbrace{\frac{d}{dt}\int_{-L_e}^{0} \rho_0 b H \bar{s}\ dx}_{S_1} = \rho_0 b H \left(\underbrace{\bar{u}\bar{s}}_{S_2} + \underbrace{\overline{u's'}}_{S_3} - \underbrace{K_h \frac{\partial \bar{s}}{\partial x}}_{S_4} \right)\Bigg|_{x=0}. \tag{23}$$

Here, it is assumed that salt transport vanishes at the upstream limit. Term S_1 represents time rate of change of salt content in the estuary, and S_2–S_4 are depth-averaged salt fluxes at the estuary mouth due to river flow, exchange flow, and horizontal diffusion, respectively. Figure 5 shows time series of the river discharge, salt intrusion lengths, and terms S_2, S_3, and S_4.

Figure 5a reveals that the adjustment of the salt intrusion length to a freshwater pulse is to a good approximation linear in time. Figure 5b shows that the magnitude of the salt flux due to exchange flow (S_3) is indeed larger during the adjustment for higher values of Q_{bg}, which slows down the adjustment. The diffusive salt flux S_4 is small compared to the other fluxes for all cases. Figures 5c and 5d reveal that higher values of U_T cause a smaller change in salt intrusion length, but that the magnitudes of the salt fluxes into the estuary during the adjustment are only slightly affected by the different value of U_T, which is in line with the results shown in Figure 4c.

Regarding the recovery time, we see that a substantial part of the recovery takes place in the first few days after the pulse (Figure 5a). This means that the salt transport due to exchange flow just after the pulse is very important

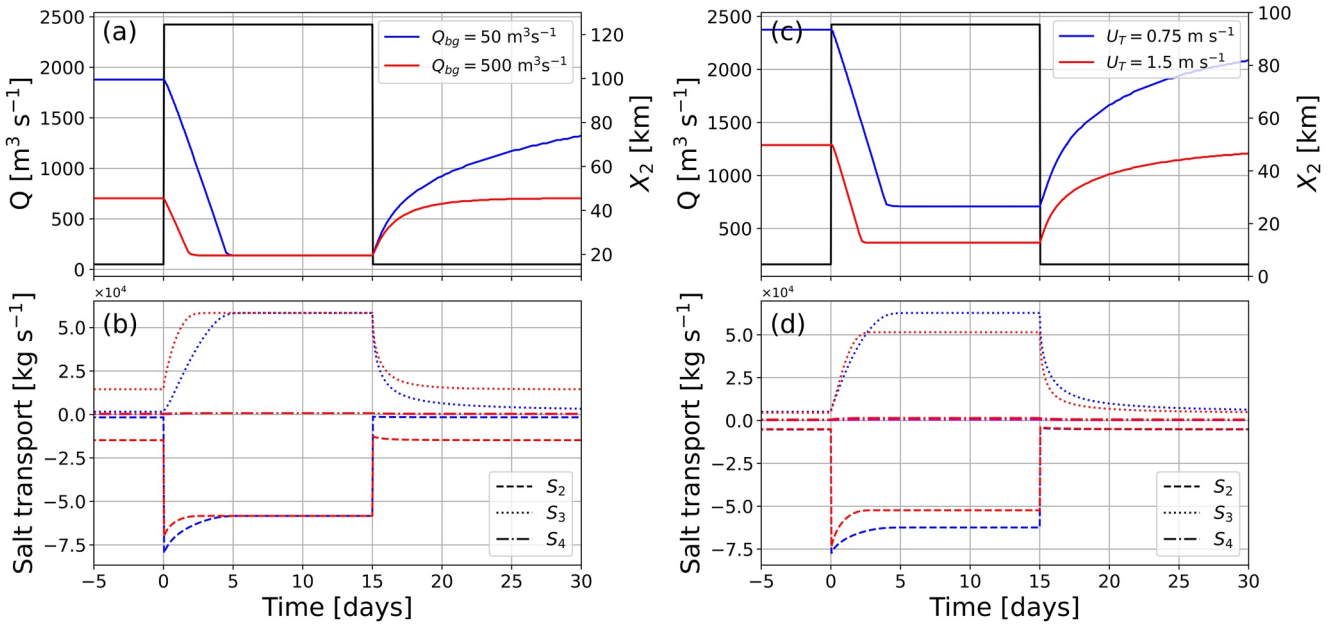

Figure 5. (a) Time series of river discharge (black line) and salt intrusion length (colored lines) for different background river discharges Q_{bg}. Only the discharge for the case $Q_{bg} = 50$ m^3 s^{-1} is plotted. These simulations are from experiment set *Background* (i.e., $Q_p = 2{,}423$ m^3 s^{-1}). (b) Time series of the different terms at the right-hand side of Equation 23. The colors refer to the same simulations as in panel (a). (c, d) As (a) and (b), except for different values of U_T. Figures similar to (a) and (c) are also in Chen (2015) and Monismith (2017), but additionally here, also the contribution of the different salt transport terms over time is displayed.

for the total recovery time. The value of $T_{rec,sc}$ is calculated by assuming this transport scales with the transport of salt by the background river flow, which is not a good estimate during this period, especially for strong pulses. Thus, T_{rec} will be shorter than $T_{rec,sc}$ for strong pulses, which is indeed found. The effect of U_T is clearly illustrated in Figures 5c and 5d: a lower value of U_T means that the change in salt intrusion length is larger (Figure 5c), but also the salt flux due to exchange flow S_3 is stronger (Figure 5d) and these effects compensate each other.

Results of experiment set *Peak* are shown in Figure 6. The same quantities as in Figure 4 are displayed, except now for different values of $Fr_{R,bg}$ and $Fr_{R,p}$, while the amplitude of the tidal current and duration of the freshwater pulse are kept fixed (Table 1). Figure 6a shows background salt intrusion lengths for reference purposes. Figures 6b and 6c show the same patterns as in experiment set *Background*: with increasing strength of the pulses,

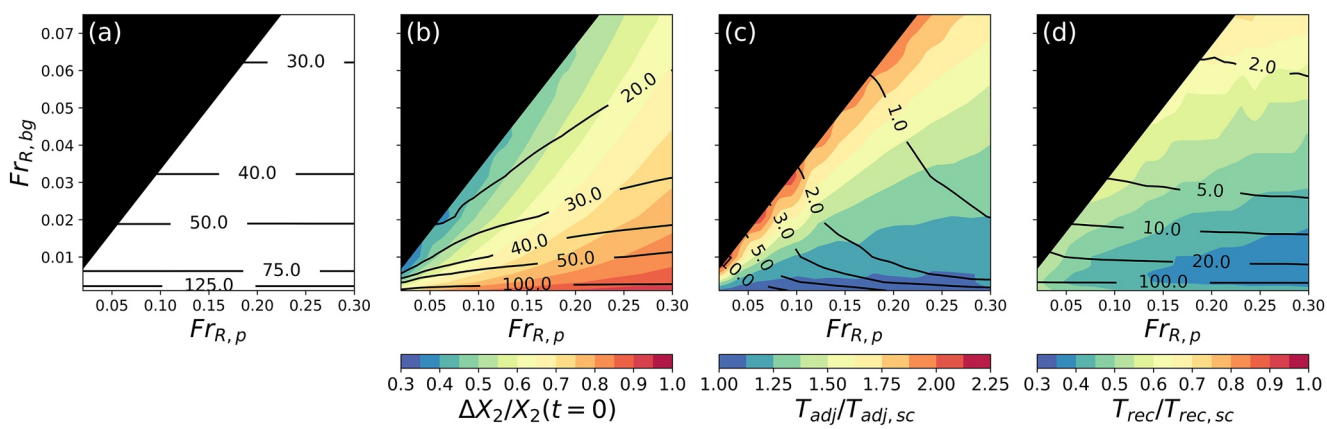

Figure 6. Results of experiment set *Peak*. (a) Contour plot of background salt intrusion length $X_2(t = 0)$ (values in km) as a function of peak freshwater Froude number $Fr_{R,p}$ and background freshwater Froude number $Fr_{R,bg}$. (b) As panel (a), except for the change in salt intrusion length ΔX_2 (contours, values in km) and the scaled change in salt intrusion length $\Delta X_2/X_2(t = 0)$ (colors). (c). As panel (b), except for the adjustment time T_{adj} (contours, values in days) and the scaled adjustment time $T_{adj}/T_{adj,sc}$ (colors). (d) As panel (c), except for the recovery time T_{rec} and the scaled recovery time $T_{rec}/T_{rec,sc}$. The black area indicates where $Fr_{R,p} < 3\ Fr_{R,bg}$.

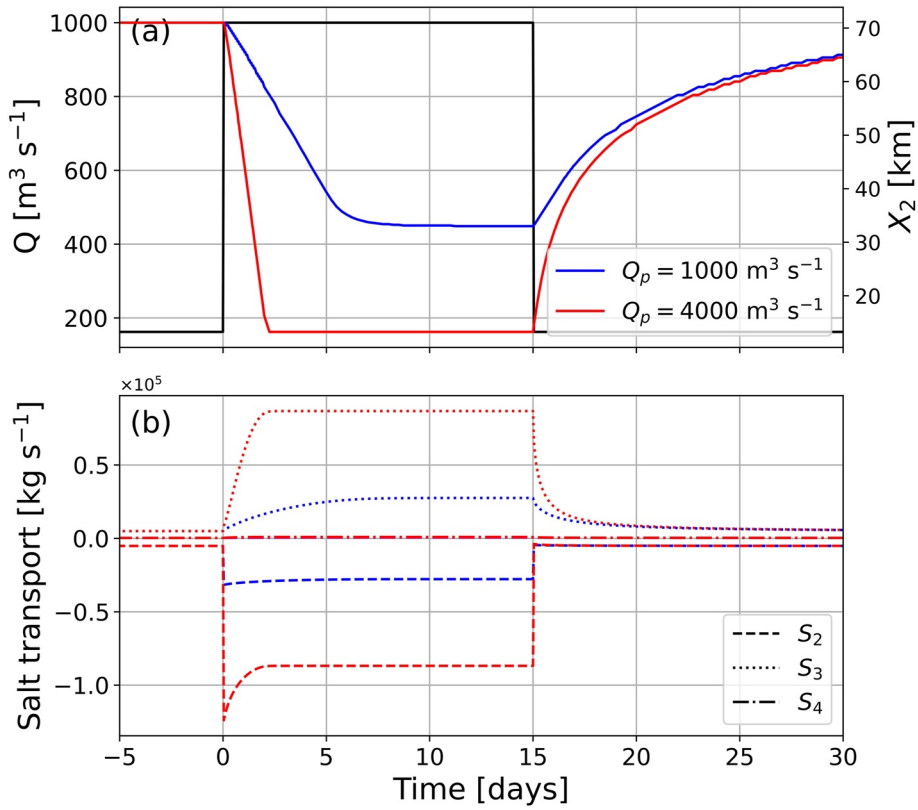

Figure 7. As Figures 5a and 5b, except for different values of peak river discharge Q_p from experiment set *Peak*. In panel (a) only the discharge for the case Q_p = 1,000 m^3 s^{-1} is plotted.

the change in salt intrusion length becomes larger and the adjustment time becomes smaller. The recovery time barely depends on the value of $Fr_{R,p}$ (Figure 6d).

The patterns in parameter space in experiment set *Background* are mostly explained by whether a pulse is "weak" or "strong," that is, from the ratio between $Fr_{R,bg}$ and $Fr_{R,p}$. Regarding the change in salt intrusion length, its dependence on $Fr_{R,p}$ follows again from the fact that

$$\Delta X_2/X_2(t=0) \sim 1 - \left(\frac{Fr_{R,bg}}{Fr_{R,p}}\right)^{\frac{1}{3}}. \tag{24}$$

This behavior is visible in Figure 6b. A least squares fit to this data yields an exponent of 0.39 ± 0.02 in this relation. The associated value of $R^2 = 0.887$ and a scatter plot displaying the performance of the fit is in Text S1 in Supporting Information S1, which indicates that the fit appropriately captures the response.

The adjustment time is close to the advective time scale for strong pulses, as is seen by values of the scaled adjustment time ($T_{rec}/T_{rec,sc}$) ≃ 1 in the lower right part of Figure 6c. For weaker pulses, the import of salt due to the exchange flow during the adjustment cannot be ignored and the adjustment is slower, leading to higher values of the scaled adjustment time when going to the left or upward in this figure.

The strong dependence of the exchange flow on the salinity gradient explains why the recovery time hardly depends on the peak river discharge. Since the salinity gradient is larger after a pulse with a high value of Q_p, the recovery due to the exchange flow will be faster. This is compensated by the larger change in salt intrusion length for a larger Q_p.

To illustrate the previous statements regarding time scales, Figure 7 displays salt intrusion lengths (Figure 7a) and S_2, S_3, and S_4 of Equation 23 (Figure 7b) for two different values of peak river discharge. Regarding the adjustment time, Figure 7b shows that during adjustment to the peak river discharge, the salt transport due to exchange

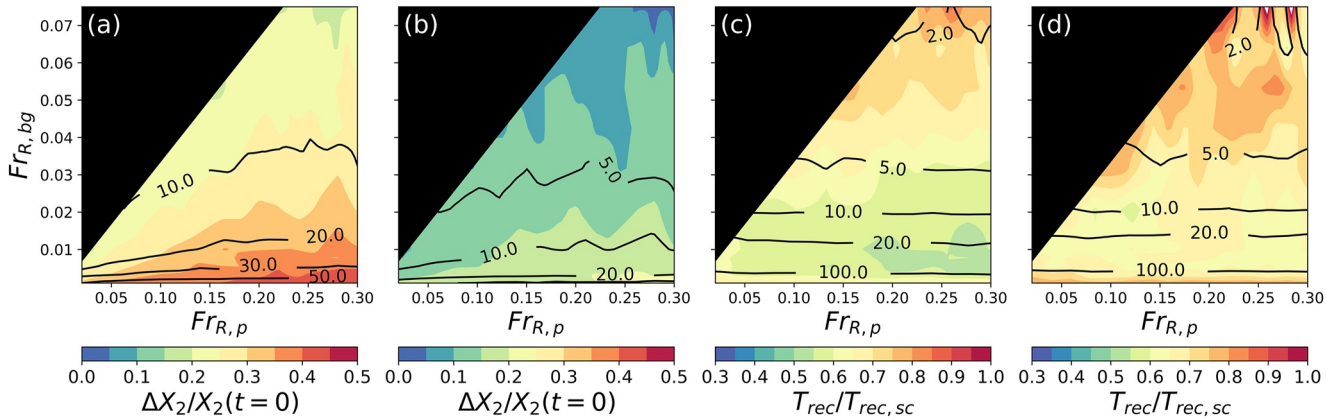

Figure 8. Results of experiment *Short*. (a) Contour plot of change in salt intrusion length ΔX_2 (contours, values in km) and scaled change in salt intrusion length $\Delta X_2/X_2(t=0)$ (colors) a function of peak freshwater Froude number $Fr_{R,p}$ and background freshwater Froude number $Fr_{R,bg}$ for $T_{pulse} = \frac{1}{2}T_{adj}$. (b) As panel (a), except for $T_{pulse} = \frac{1}{4}T_{adj}$. (c) As panel (a), except for the recovery time T_{rec} (contours, values in days) and the scaled recovery time $T_{adj}/T_{adj,sc}$ (colors). (d) As panel (c), except for $T_{pulse} = \frac{1}{4}T_{adj}$. The black area indicates where $Fr_{R,p} < 3\ Fr_{R,bg}$.

flow (S_3) is relatively stronger for the weaker pulse. The rate of recovery immediately after the pulse is higher for the larger pulse, leading to a similar situation for both cases after a few days and thus pulses with different strengths have approximately the same recovery time.

Finally, results for experiment set *Short* are displayed in Figure 8. Figures 8a and 8b show the values of change in salt intrusion length for different values of $Fr_{R,p}$ and $Fr_{R,bg}$ and for two durations of the pulse, with Fr_T fixed. It appears that the change in salt intrusion length depends approximately linearly on the duration of the pulse. This is the case for all values of $Fr_{R,p}$ and $Fr_{R,bc}$. Figures 8c and 8d show that the recovery time T_{rec} barely depends on the duration of the pulse.

The linear dependence of ΔX_2 on T_{pulse} is a consequence of the fact that the time rate of change of X_2 is linear in time during most of the adjustment (Figures 5 and 7). Thus, the change in salt intrusion length can be estimated from multiplying the downstream velocity of the salt intrusion with the duration of the pulse. Because of this, ΔX_2 will indeed depend linearly on T_{pulse} when no equilibrium is reached.

The finding that T_{rec} does not depend on T_{pulse} is due to the fact that the exchange flow is not fully developed before equilibrium with the peak discharge is reached (see Figures 5 and 7). When the pulse ends at this stage, salt import will thus be weaker compared to when the pulse would have reached equilibrium. So during the recovery after a shorter pulse, the upstream velocity of the salt intrusion will be smaller. At the same time, ΔX_2 is also smaller for shorter pulses. These two effects have similar magnitude and will compensate each other.

3.2. Specific Application

In this section, the model performance is assessed by applying it to observed freshwater pulses in the Guadalquivir Estuary and comparing the model simulations with observations in this estuary. For this purpose, the model was slightly extended to a new geometry that consists of multiple (instead of one) estuarine parts, as is shown in Figure 9. In each of these parts, the equations as presented in Section 2.2 are solved. For salinity, the matching conditions shown in Equation 11 are used at the boundaries of the parts. Furthermore, additional river discharge of four tributaries are added at the beginning of each part. The other model settings are equal to those used in Section 2.3, with one exception: for salinity at the river boundary, a value of 0.5 psu was used, based on observations.

Details about the observations are given in Navarro et al. (2011, 2012). To determine the subtidal salt intrusion length, first a Gaussian filter with a half-amplitude of 12 hr is applied to the raw salinity measurements to average over the tides. Afterward, the observed salinity (observations are done at the surface) is linearly interpolated between the measurement points and the most upstream point where the salinity exceeds 2 psu is identified.

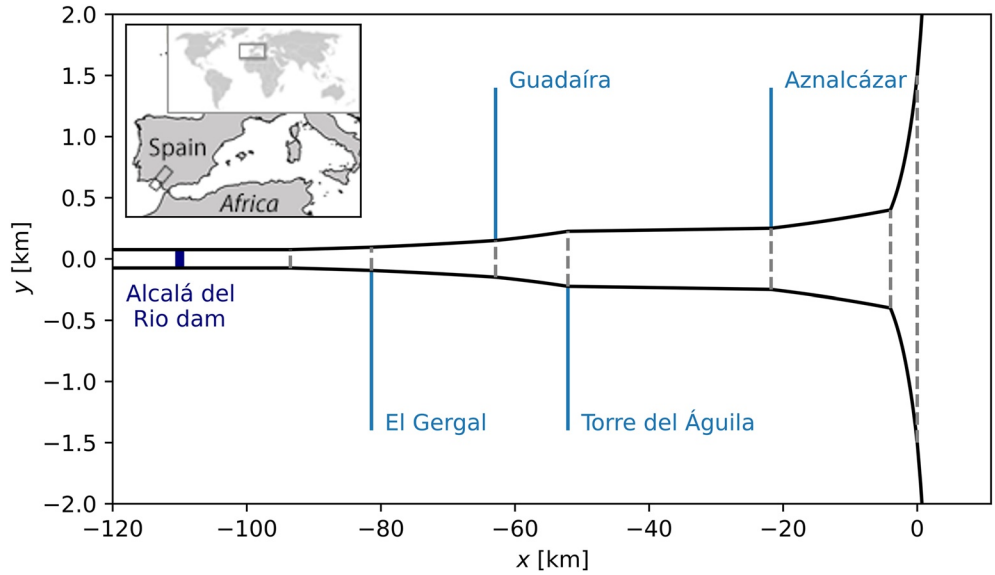

Figure 9. The geometry of the Guadalquivir Estuary used for the simulation. The most upstream and downstream domains are not entirely plotted, because of their extent in the *x*- and *y*-direction, respectively.

During the observational period, several freshwater pulses occurred: one in February 2009 and a series of three pulses in 2010.

Simulations are done in order to capture the effects of these pulses. Figure 10 displays the results of these simulations and the observations in the Guadalquivir. A more detailed analysis of the model performance regarding simulation of salt intrusion length and the spatial structure of the salt field is given in Text S2 in Supporting Information S1. The results demonstrate that the spatial structure of the salt field is fairly well simulated. To quantify the differences, the root-mean-square error of the observed and simulated salt intrusion length is calculated, which will be noted as RMSE(X_2). For the 2009 case, RMSE(X_2) = 9.6 km. However, this number does not reflect the temporal differences: before day 50 of the year 2009, RMSE(X_2) = 3.7 km and after this date it is 15.7 km. For the simulations of the pulses in 2010, we have RMSE(X_2) = 5.4 km. These values indicate that the model is capable of simulating the temporal behavior of the salt intrusion length in the Guadalquivir Estuary during freshwater pulses. Clearly, there are differences between simulated and observed salt intrusion length, which could be reduced by applying detailed model tuning. For example, Wang et al. (2014) and Losada et al. (2017) argued that the 2009 freshwater pulse in the Guadalquivir created a mud layer on the bottom of the estuary, which decreased

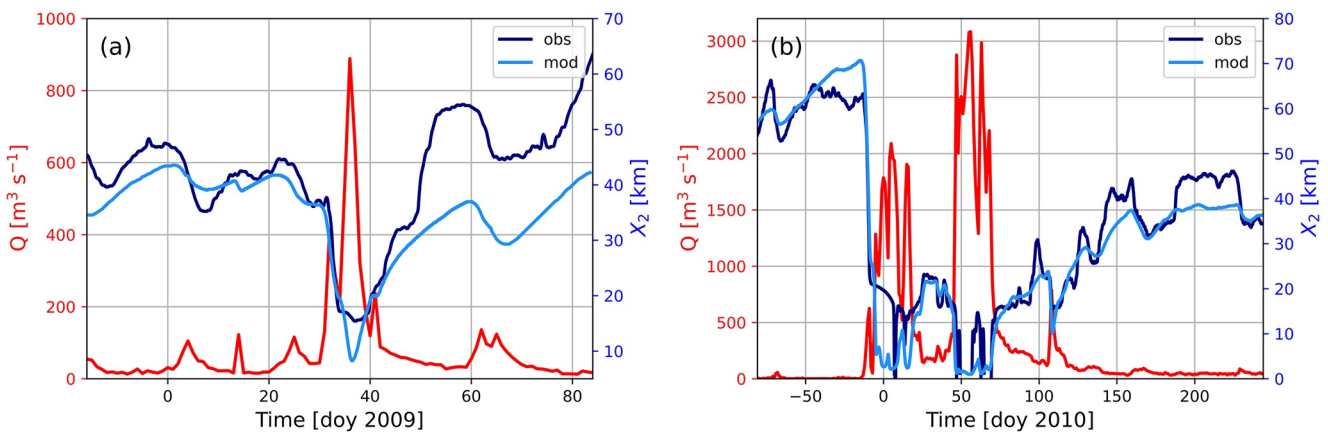

Figure 10. Time series of observed river discharge Q and observed and simulated salt intrusion length X_2 for the Guadalquivir Estuary. The discharge (the red line) is the sum of the main river plus the four tributaries. The dark blue line is the observed X_2 and the light blue line is the simulated X_2. (a) For the freshwater pulse in 2009. (b) For the series of freshwater pulses in 2010.

the hydraulic drag. This effect could be taken into account by adjusting the value of the partial slip parameter after the pulse.

3.3. Other Remarks

An interesting difference between the results presented here and existing literature concerns the recovery time. Here, we find that this quantity depends only on the river discharge during the recovery, whereas in previous studies (Chen, 2015; Kranenburg, 1986), it is stated that it depends on the change in salt intrusion length. The reason for this difference is that Kranenburg (1986) assumes that during the recovery the exchange flow does not vary in time. However, here we show that the evolution in time of the exchange flow during the recovery is important for the recovery time (Figures 5 and 7). Chen (2015) accounts of time-varying exchange flow, but he estimates recovery time from linearized equations, thereby assuming small changes in exchange flow. Our study, on the other hand, clearly shows that these changes are large. A more detailed comparison with the results of Chens theory is placed in the Text S3 in Supporting Information S1, indicating that Chens theory underpredicts the recovery time by a significant amount, which was also demonstrated by Monismith (2017).

Finally, we remark that the estuarine salt response to pulses with a duration that is shorter than the adjustment time scale of the system is not considered in the existing literature. We find that the change in salt intrusion length is linearly related to the duration of the pulse (Figure 8). This is relevant in real estuaries. The duration of freshwater pulses in the observational data sets can be compared to the theoretical adjustment time given by our model. In some of the estuaries analyzed, only a small portion of the freshwater pulses will not reach equilibrium (Mitchell River: 0.19; Tagus: 0.30; San Francisco Bay: 0.34), while in other estuaries about half of the pulses do not reach the equilibrium state (Guadalquivir: 0.41; Guadiana: 0.48). Finally, this ratio is 0.75 in the Gironde. So the duration of the pulse is often the limiting factor for the change in salt intrusion length.

3.4. Model Limitations

The idealized model used in this study is by its nature simplified and does not take all physical processes affecting salinity in estuaries into account. One limitation is that in the sensitivity analyses, a constant width and depth are used. However, real estuaries have widths and depths that vary, and this affects their response to time-varying forcing (Chen, 2017). Another simplification is that the viscosity and diffusivity coefficients are chosen to be constant in space and time. In reality, vertical mixing will depend on a lot of parameters, including stratification (Burchard et al., 2011; Monismith et al., 2002; Vaz et al., 1989). An increase in river discharge will increase the stratification in an estuary, which will decrease the strength of vertical mixing. In Text S4 in Supporting Information S1, a rough analysis of the magnitude of this effect is performed, which indicates that the values of A_v and K_v can reduce by a factor of 2–5 during a freshwater pulse. When this effect would be taken into account, increased stratification during the freshwater pulse would decrease the amount of salt being flushed out by the river discharge and the change in salt intrusion length would be smaller. A first estimate of this effect on the salt intrusion length is done in Text S4 in Supporting Information S1. In this case, the salt intrusion length changes by 13% when the Munk–Anderson parametrization (Dyer, 1973; Munk & Anderson, 1948) is used to estimate the vertical diffusivity and viscosity coefficient. A more detailed analysis of the effect of stratification dependent mixing on the salinity response to freshwater pulses is left for future study.

4. Conclusions

The aim of this study was to quantify the dependence of the estuarine salinity response to freshwater pulses to the background conditions, the intensity, and the duration of the pulse. Application of the MacCready (2007) model, which relies on the Pritchard balance, to observed freshwater pulses in the Guadalquivir Estuary showed that use of this balance results in negative salinity values. We therefore developed a new model, which uses a more detailed description of the vertical salinity structure. Simulations with this model did not show negative salinity and moreover, the model performs well when applied to observed freshwater pulses.

Model simulations revealed that the influence of the background conditions on the salinity response to a given freshwater pulse is mainly through the background river discharge; the strength of the tides is of minor importance. Changes in salt intrusion length ΔX_2 can be estimated successfully from classical theory, but this theory

is incorrect regarding adjustment time T_{adj} for weak pulses and recovery time T_{rec} for strong pulses. Simulations with different strengths of the peak river discharge revealed that for ΔX_2 the ratio of peak to background river discharge determines the response. Interestingly, the peak river discharge is the most important control for T_{adj}, while for T_{rec} its value is not important. When the duration of the freshwater pulse is too small to reach equilibrium, ΔX_2 will be linearly related to the duration of the pulse, but T_{rec} is not affected. Observed freshwater pulse characteristics indicate that this control on ΔX_2 is important in real estuaries. The results found in this study can be used to estimate the response of a given estuary to freshwater pulses when the relevant dimensionless numbers are known. Also the changes in this response when adjusting certain properties of an estuary, for instance by ship channel dredging or flow regulation, can be determined.

Data Availability Statement

Software used to generate the data and create the figures used in this study can be found at git.science.uu.nl/w.y.biemond/code-and-data-freshwater-pulses.git, as well as the river discharge data sets used. Observational data of the Guadalquivir Estuary can be found at zenodo.org/record/3459610.

Acknowledgments
This work is part of the Perspectief Program SaltiSolutions, which is financed by NWO Domain Applied and Engineering Sciences (2022/TTW/01344701) in collaboration with private and public partners. This work is also supported by Programa Estatal de Investigación (P18-32project5) and Desarrollo e Innovación orientada a los RETOS de la sociedad (CTM2017-89531-R).

References

Banas, N. S., Hickey, B. M., MacCready, P., & Newton, J. A. (2004). Dynamics of Willapa Bay, Washington: A highly unsteady, partially mixed estuary. *Journal of Physical Oceanography*, *34*(11), 2413–2427. https://doi.org/10.1175/JPO2637.1

Burchard, H., Hetland, R. D., Schulz, E., & Schuttelaars, H. M. (2011). Drivers of residual estuarine circulation in tidally energetic estuaries: Straight and irrotational channels with parabolic cross section. *Journal of Physical Oceanography*, *41*(3), 548–570. https://doi.org/10.1175/2010JPO4453.1

Canuto, C., Hussaini, M. Y., Quarteroni, A., & Zang, T. A., Jr. (2012). *Spectral methods in fluid dynamics*. Springer Science & Business Media. https://doi.org/10.1137/1030157

Chatwin, P. (1976). Some remarks on the maintenance of the salinity distribution in estuaries. *Estuarine and Coastal Marine Science*, *4*(5), 555–566. https://doi.org/10.1016/0302-3524(76)90030-X

Chen, S.-N. (2015). Asymmetric estuarine responses to changes in river forcing: A consequence of nonlinear salt flux. *Journal of Physical Oceanography*, *45*(11), 2836–2847. https://doi.org/10.1175/JPO-D-15-0085.1

Chen, S.-N. (2017). Bathymetric influences on the estuarine equilibrium length and adjustment time. *Journal of Physical Oceanography*, *47*(7), 1719–1736. https://doi.org/10.1175/JPO-D-16-0075.1

Crank, J., & Nicolson, P. (1947). A practical method for numerical evaluation of solutions of partial differential equations of the heat-conduction type. *Mathematical Proceedings of the Cambridge Philosophical Society*, *43*, 50–67. https://doi.org/10.1017/S0305004100023197

Díez-Minguito, M., Contreras, E., Polo, M., & Losada, M. (2013). Spatio-temporal distribution, along-channel transport, and post-riverflood recovery of salinity in the Guadalquivir Estuary (SW Spain). *Journal of Geophysical Research: Oceans*, *118*, 2267–2278. https://doi.org/10.1002/jgrc.20172

Dijkstra, Y. M., & Schuttelaars, H. M. (2021). A unifying approach to subtidal salt intrusion modeling in tidal estuaries. *Journal of Physical Oceanography*, *51*(1), 147–167. https://doi.org/10.1175/JPO-D-20-0006.1

Du, J., & Park, K. (2019). Estuarine salinity recovery from an extreme precipitation event: Hurricane Harvey in Galveston Bay. *Science of the Total Environment*, *670*, 1049–1059. https://doi.org/10.1016/J.SCITOTENV.2019.03.265

Du, J., Park, K., Dellapenna, T. M., & Clay, J. M. (2019). Dramatic hydrodynamic and sedimentary responses in Galveston Bay and adjacent inner shelf to Hurricane Harvey. *Science of the Total Environment*, *653*, 554–564. https://doi.org/10.1016/j.scitotenv.2018.10.403

Dyer, K. R. (1973). *Estuaries: A physical introduction*. John Wiley.

Galántai, A. (2000). The theory of Newton's method. *Journal of Computational and Applied Mathematics*, *124*(1–2), 25–44. https://doi.org/10.1016/S0377-0427(00)00435-0

Geyer, W. R., & MacCready, P. (2014). The estuarine circulation. *Annual Review of Fluid Mechanics*, *46*, 175–197. https://doi.org/10.1146/annurev-fluid-010313-141302

Gong, W., Shen, J., & Reay, W. G. (2007). The hydrodynamic response of the York River estuary to Tropical Cyclone Isabel, 2003. *Estuarine, Coastal and Shelf Science*, *73*(3), 695–710. https://doi.org/10.1016/j.ecss.2007.03.012

Guerra-Chanis, G. E., So, S., & Valle-Levinson, A. (2021). Effects of Hurricane Irma on residual flows and saltwater intrusion in a subtropical estuary. *Regional Studies in Marine Science*, *41*, 101568. https://doi.org/10.1016/j.rsma.2020.101568

Guha, A., & Lawrence, G. A. (2013). Estuary classification revisited. *Journal of Physical Oceanography*, *43*(8), 1566–1571. https://doi.org/10.1175/JPO-D-12-0129.1

Hansen, D. V., & Rattray, M. (1965). Gravitational circulation in straits and estuaries. *Journal of Marine Research*, *23*, 104–122. https://doi.org/10.1357/002224021834614399

Hansen, D. V., & Rattray, M. (1966). New dimensions in estuary classification 1. *Limnology & Oceanography*, *11*(3), 319–326. https://doi.org/10.4319/lo.1966.11.3.0319

Hetland, R. D., & Geyer, W. R. (2004). An idealized study of the structure of long, partially mixed estuaries. *Journal of Physical Oceanography*, *34*(12), 2677–2691. https://doi.org/10.1175/JPO2646.1

Ingram, R., d'Anglejan, B., Lepage, S., & Messier, D. (1986). Changes in current regime and turbidity in response to a freshwater pulse in the Eastmain estuary. *Estuaries*, *9*(4), 320–325. https://doi.org/10.2307/1351411

Kranenburg, C. (1986). A time scale for long-term salt intrusion in well-mixed estuaries. *Journal of Physical Oceanography*, *16*(7), 1329–1331. https://doi.org/10.1175/1520-0485(1986)016<1329:ATSFLT>2.0.CO;2

Lepage, S., & Ingram, R. G. (1988). Estuarine response to a freshwater pulse. *Estuarine, Coastal and Shelf Science*, *26*(6), 657–667. https://doi.org/10.1016/0272-7714(88)90041-8

Liu, W.-C., Chen, W.-B., & Kuo, J.-T. (2008). Modeling residence time response to freshwater discharge in a mesotidal estuary, Taiwan. *Journal of Marine Systems*, *74*(1–2), 295–314. https://doi.org/10.1016/j.jmarsys.2008.01.001

Losada, M., Díez-Minguito, M., & Reyes-Merlo, M. (2017). Tidal–fluvial interaction in the Guadalquivir River Estuary: Spatial and frequency-dependent response of currents and water levels. *Journal of Geophysical Research: Oceans*, *122*, 847–865. https://doi.org/10.1002/2016JC011984

MacCready, P. (2004). Toward a unified theory of tidally-averaged estuarine salinity structure. *Estuaries*, *27*(4), 561–570. https://doi.org/10.1007/BF02907644

MacCready, P. (2007). Estuarine adjustment. *Journal of Physical Oceanography*, *37*(8), 2133–2145. https://doi.org/10.1175/JPO3082.1

McFarland, K., Rumbold, D., Loh, A. N., Haynes, L., Tolley, S. G., Gorman, P., et al. (2022). Effects of freshwater release on oyster reef density, reproduction, and disease in a highly modified estuary. *Environmental Monitoring and Assessment*, *194*(2), 1–30. https://doi.org/10.1007/s10661-021-09489-x

Monismith, S. (2017). An integral model of unsteady salinity intrusion in estuaries. *Journal of Hydraulic Research*, *55*(3), 392–408. https://doi.org/10.1080/00221686.2016.1274682

Monismith, S., Kimmerer, W., Burau, J., & Stacey, M. (2002). Structure and flow-induced variability of the subtidal salinity field in northern San Francisco Bay. *Journal of Physical Oceanography*, *32*(11), 3003–3019. https://doi.org/10.1175/1520-0485(2002)032<3003:SAFIVO>2.0.CO;2

Munk, W., & Anderson, R. (1948). Notes on the theory of the thermocline. *Journal of Marine Research*, *7*, 276–295.

Navarro, G., Gutiérrez, F. J., Díez-Minguito, M., Losada, M. A., & Ruiz, J. (2011). Temporal and spatial variability in the Guadalquivir Estuary: A challenge for real-time telemetry. *Ocean Dynamics*, *61*(6), 753–765. https://doi.org/10.1007/s10236-011-0379-6

Navarro, G., Huertas, I. E., Costas, E., Flecha, S., Díez-Minguito, M., Caballero, I., et al. (2012). Use of a real-time remote monitoring network (RTRM) to characterize the Guadalquivir Estuary (Spain). *Sensors*, *12*(2), 1398–1421. https://doi.org/10.3390/s120201398

Paerl, H. W., Valdes, L. M., Joyner, A. R., Peierls, B. L., Piehler, M. F., Riggs, S. R., et al. (2006). Ecological response to hurricane events in the Pamlico Sound system, North Carolina, and implications for assessment and management in a regime of increased frequency. *Estuaries and Coasts*, *29*(6), 1033–1045. https://doi.org/10.1007/BF02798666

Pritchard, D. W. (1954). A study of the salt balance in a coastal plain estuary. *Journal of Marine Research*, *13*(1), 133–144.

Ralston, D. K., Geyer, W. R., & Lerczak, J. A. (2008). Subtidal salinity and velocity in the Hudson River estuary: Observations and modeling. *Journal of Physical Oceanography*, *38*(4), 753–770. https://doi.org/10.1175/2007JPO3808.1

Tee, K.-T., & Lim, T.-H. (1987). The freshwater pulse—A numerical model with application to the St. Lawrence Estuary. *Journal of Marine Research*, *45*(4), 871–909. https://doi.org/10.1357/002224087788327127

Valle-Levinson, A., Wong, K.-C., & Bosley, K. T. (2002). Response of the lower Chesapeake Bay to forcing from Hurricane Floyd. *Continental Shelf Research*, *22*(11), 1715–1729. https://doi.org/10.1016/S0278-4343(02)00034-1

Vaz, R. A. N., Lennon, G. W., & de Silva Samarasinghe, J. R. (1989). The negative role of turbulence in estuarine mass transport. *Estuarine, Coastal and Shelf Science*, *28*(4), 361–377. https://doi.org/10.1016/0272-7714(89)90085-1

Wang, Z. B., Winterwerp, J. C., & He, Q. (2014). Interaction between suspended sediment and tidal amplification in the Guadalquivir Estuary. *Ocean Dynamics*, *64*(10), 1487–1498. https://doi.org/10.1007/s10236-014-0758-x